Electronic Supplementary Information:

Can Cr(III) substitute for Al(III) in the structure of Boehmite?

Sayandev Chatterjee,[a]* Michele A. Conroy,[a] Frances N. Smith,[a] Hee-Joon Jung,[a] Z. Wang,[b] Reid A. Peterson,[a] Ashfia Huq,[c] David G. Burtt,[a] Eugene S. Ilton,[b]* Edgar C Buck[a]*

[a] *Energy and Environment Directorate, Pacific Northwest National Laboratory, Richland, WA 99354, United States.*
[b] *Physical and Computational Sciences Directorate, Pacific Northwest National Laboratory, Richland, WA 99354, United States.*
[c] *Chemical and Engineering Materials Division, Oak Ridge National Laboratory, Oak Ridge, Tennessee 37831, United States.*

X-ray diffraction (XRD): XRD patterns of the samples were recorded on a Philips X'pert Multi-Purpose Diffractometer (MPD) (PANAlytical, Almelo, The Netherlands) equipped with a fixed Cu anode operating at 45 kV and 40 mA. XRD patterns were collected in the 5-100° 2θ-range with 0.04° steps at a rate of 5 s/step. Phase identification was performed using JADE 9.5.1 from Materials Data Inc., and the 2012 PDF4+ database from International Center for Diffraction Data (ICDD) database.[1]

Time-of-flight (TOF) neutron diffraction: Diffraction data over d range of 0.1 to 8.5 Å were collected with the POWGEN powder diffractometer at the Spallation Neutron Source of Oak Ridge National Laboratory (ORNL). Measurements were made at 300 K. Rietveld refinement was performed using the software package GSAS.[2,3]

FTIR spectroscopy*: Measurements* were conducted using a spectrometer (ALPHA model, Bruker Optics) operated with OPUS software (Version 6.5 Build 6.5.92). Samples were run directly on a diamond attenuated total reflectance (ATR) cell. For each sample, 24 scans with a resolution of 4 wavenumbers (cm^{-1}) were averaged to give the final spectrum. A background of ambient air was used for all samples.

Raman spectroscopy: *Measurements* were performed with an InPhotonics RS2000 Raman spectrometer containing a thermoelectrically cooled charge-coupled device (CCD) detector operating at −55 °C. A 670 nm, 150-mW, visible diode laser was used as the excitation source, and a focused fiber-optic InPhotonics Raman probe was operated in a 180°-back reflection mode. The laser beam focal point was 5 mm beyond the end of the laser probe quartz window and into the interrogated solid samples. The measured laser intensity at the sample was typically 50 mW. Raman spectra were acquired from all the samples at room temperature (20.4−20.9 °C). For each sample, an integration time of 10 s was used for each acquisition, and 10 acquisitions were averaged per sample.

Excitation and emission spectroscopy: Steady state excitation and emission spectra were recorded using a Horizon Fluorolog III fluorimeter equipped with a 450 W Xenon lamp and both R928 and liquid nitrogen cooled R5509 Hamamatsu photomultiplier tubes. Time resolved excitation and emission spectra were recorded using an instrument equipped with a double-emission monochromator and a single-excitation monochromator. Emission spectra were corrected for instrumental response except where noted. Samples in 2 mm × 4 mm quartz cuvettes were mounted on the sample holder of a CRYO Industries RC152 cryostat. The sample was excited with a Spectra-Physics Nd:YAG laser-pumped MOPO-730 laser, and the emitted light was collected at 85˚ to the excitation beam, dispersed through an Acton SpectroPro 300i double-monochromator spectrograph, and detected with a thermoelectrically cooled, Princeton Instruments PIMAX intensified CCD camera. Solid samples for emission were contained in a silica cell.

***X-ray photoelectron spectroscopy (XPS)*:** Samples in the form of powder were pressed with clean borosilicate glass blocks onto copper stubs that were covered with a strip of conductive copper tape. All preparation occurred under

atmospheric conditions. XPS measurements were performed with a Kratos Axis Ultra DLD spectrometer that employs a monochromatic Al *Kα* X-ray (1486.7 eV) source operating at 10mA and 15 kV. Collection efficiency was enhanced by use of a magnetic immersion lens. The instrument work function was calibrated to give a BE of 83.96 eV ± 0.05 eV for the $4f_{7/2}$ line of metallic gold and the spectrometer dispersion was adjusted to give a BE of 932.62 eV for the Cu$2p_{3/2}$ line of metallic copper. High resolution measurements of Al*2p*, Cr*2p*, O*1s*, and C*1s* were performed with an analysis area of 300 x 700 microns, a step size of 0.1eV, and pass energies (PE) of 40 eV which produced a full-width-at-half- maximum (FWHM) for the Ag$3d_{5/2}$ line of 0.77 eV, respectively. Survey scans were performed at PE = 160 eV and step size = 0.5 eV. Spectra were best fit, after Shirley background subtractions, by non-linear least squares using the CasaXPS curve resolution software package. Gaussian/Lorentzian (G/L) contributions to the line shapes were numerically convoluted using a Voigt function. Instrument-specific sensitivity factors were used for quantification. An electron flood gun was required to minimize sample charging.

***TEM and SEM*:** SEM was performed with a FEI (Hillsboro, OR, USA) Helios 660 NanoLab™ dual-beam Scanning Electron Microscope (SEM) with a Focused Ion Beam (FIB) equipped with an EDAX (EDAX Inc., Mahwah, NJ) compositional analysis system. Samples for both SEM and TEM were deposited as fine powders onto a holey carbon copper-grid. In the SEM, imaging was performed in transmission High Angle Annular Dark Field (HAADF) mode (using the FEI STEM-3+ detector) and with secondary electron imaging. Selected specimens were ion-beam sectioned using the SEM-FIB and mounted on Omniprobe lift-out grids (Electron Microscopy Sciences, Hatfield, PA) for analysis in the Transmission Electron Microscope. TEM work was performed using a JEOL ARM200F (JEOL, Peabody, MA) operated at 200 keV and equipped with a Noran™ (Thermo Scientific, Waltham, MA) EDS system and a FEI Titan 30-800 operated at 300 keV and equipped with a Gatan™ (Gatan, Inc., Pleasanton, CA) Image Filter. Electron energy loss images were obtained by collecting EELS spectra in STEM mode. Spectrum-Image files were analyzed using the custom Spectrum Image (SI) script package developed by Mitchell.[4] Images showing the occurrence of Cr utilized the Cr-$L_{2,3}$ absorption edges and the O-K edge. Because of the proximity of these edges, routine background subtraction methods were ineffective. Elemental mapping with EDS using the Al and Cr x-ray lines was also used but this technique has poorer spatial resolution than EELS. Diffraction patterns and electron micrographs were analyzed with Gatan Digital Micrograph™ 3.01 and aided with simulated diffraction patterns generated using CrystalMaker®2.2, a crystal and molecular structures program for Mac and Windows, and SingleCrystal®2.0.1, an electron diffraction simulation program distributed by Crystal Maker Software Ltd., Oxford, England (http://www.crystalmaker.com).

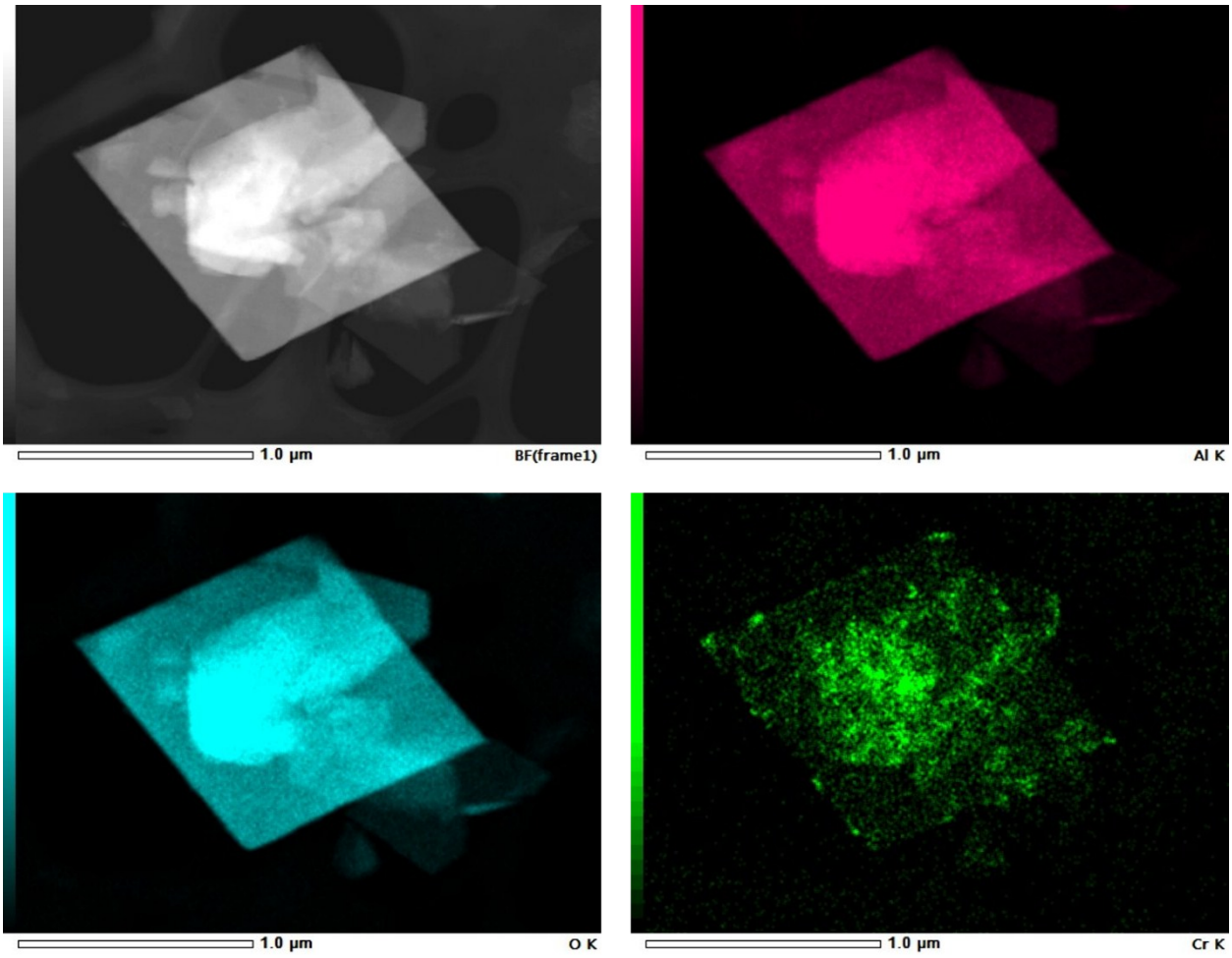

S1 STEM EDS mapping for the key elements (Al, O, Cr) for the 10% Cr(III) doped rhombic plates **1-Cr$_b$**.

Incorporation Energy Calculations

Boehmite supercells were generated in order to evaluate experimentally relevant weight percentages of Cr associated with this phase (e.g., 1-10 wt. % Cr). Specifically, a 4×1×4 boehmite supercell was generated containing 256 atoms where the substitution of 1 Cr(III) for 1 Al(III) is 1.3 wt. % Cr. For both bulk and slab models, incorporation energies (E_{inc}) were calculated using a generalized "Products-minus-reactants" approach, as illustrated in the following equations for bulk (Equation S1) and surface slab (Equation S2) environments:

$$E_{\text{inc-bulk}} = (E_{\text{defect-bulk}} + E_{\text{Al(III),gas}}) - (E_{\text{pure-bulk}} + E_{\text{Cr(III),gas}}) \quad \textbf{Equation S1}$$

$$E_{\text{inc-slab}} = (E_{\text{defect-slab}} + E_{\text{Al(III),gas}}) - (E_{\text{pure-slab}} + E_{\text{Cr(III),gas}}) \quad \textbf{Equation S2}$$

Here, $E_{\text{defect-bulk}}$ and $E_{\text{pure-bulk}}$ refer to the energies of Cr-doped and non-Cr doped boehmite supercells, respectively, that are treated as infinite in three dimensions. Similarly, $E_{\text{defect-slab}}$ and $E_{\text{pure-slab}}$ refer to energies of Cr-doped and non-Cr-doped boehmite slabs, respectively, that are treated as infinite in two dimensions (*i.e.,* in the *xy* plane) but not perpendicular to the surface (*i.e.,* the *z* direction). Energies of the ionic species that are added or removed from the bulk (*e.g.,* $E_{\text{Cr(III),gas}}$) and $E_{\text{Al(III),gas}}$, respectively) are calculated as ions in a vacuum. Ionization energies going from Al^0 to Al(III) and Cr^0 to Cr(VI) are calculated and compared with experimental data to assess the accuracy of these reference points (Table S1).

Table S1. Calculated ionization energies versus experimental ionization energies

Ionic State	Electron Configuration	Opt E / atom (Ha)	Opt E / atom (eV)	Calc. I.E. (eV/atom)	Exper.* (eV/atom)	Ionization Step	% Difference
Al^0	$[Ne]3s^23p^1$	-241.7796	-6579.0645	---	---	---	---
Al^{1+}	$[Ne]3s^2$	-241.6466	-6575.4470	3.62	5.99	First	-39.56
Al^{2+}	$[Ne]3s^1$	-241.0203	-6558.4036	17.04	18.83	Second	-9.48
Al^{3+}	$1s^22s^2sp^6$	-239.9913	-6530.4038	28.00	28.45	Third	-1.57
Cr^0	$[Ar]3d^54s^1$	-1042.2106	-28359.5924	---	---	---	---
Cr^{1+}	$[Ar]3d^5$	-1043.0733	-28383.0669	-23.47	6.77	First	-446.92
Cr^{2+}	$[Ar]3d^4$	-1042.5381	-28368.5054	14.56	16.49	Second	-11.68
Cr^{3+}	$[Ar]3d^3$	-1041.3807	-28337.0110	31.49	30.96	Third	1.73
Cr^{4+}	$[Ar]3d^2$	-1039.6658	-28290.3466	46.66	49.16	Fourth	-5.08
Cr^{5+}	$[Ar]3d^1$	-1037.1347	-28221.4720	68.87	69.46	Fifth	-0.84
Cr^{6+}	$[Ne]3s^23p^6$	-1033.8371	-28131.7414	89.73	90.63	Sixth	-1.00

Ionization energies from Kramida, A., Ralchenko, Y., Reader, J. and NIST ASD Team (2014)

NIST Atomic Spectra Database (ver. 5.2), [Online]. Available: http://physics.nist.gov/asd

National Institute of Standards and Technology, Gaithersburg, MD.

Here, differences in calculated versus experimental ionization energies decrease as the Al(III) and Cr(III) oxidation states are approached, attributed to the oxidation states for which the basis sets were optimized.[5,6] While not performed here, hydration energy corrections can be applied to calculation of the gas-phase ionic species to relate energy values more closely to real-world, environmentally relevant conditions, as described in previous publications.[7,8] In all cases, the incorporation of the defect element is interpreted to be favorable if E_{inc} is negative, and an energy barrier to incorporation is interpreted to exist if E_{inc} are positive. It is important to note that the bulk, slab, and gas-phase energies are calculated at zero Kelvin; however, hydration energy corrections do account for a room-temperature normalization.

Surface Energy Calculations

Surface energy calculations were performed in conjunction with slab incorporation energies to evaluate the relative reactivity of different low-index terminations of boehmite. Specifically, surface energies were calculated for the (010), (100), and (001) surfaces of boehmite with $P2_1/b$ symmetry. **Equation S3** below was used to calculate the surface energy of the slabs (after Skomurski et al., 2006):[9]

$$E_{surf} = \left(E_{slab} - \left(\frac{\#\ atoms\ in\ slab}{\#\ atoms\ in\ bulk}\right) \cdot E_{bulk}\right) \cdot \left(\frac{1}{2 \cdot slab\ surf.\ area}\right) \cdot \left(\frac{1.602 \cdot 10^{-19} J/eV}{1 \cdot 10^{-20}\, m^2/Å^2}\right)$$

Equation S3

Here, E_{surf} is the calculated energy of a single surface of the slab, when the energy of the two-dimensionally infinite slab model (E_{slab}) is normalized to the energy of the three-dimensionally infinite bulk model (E_{bulk}) by taking a ratio of the number of atoms in one model versus the other, respectively. The net energy is divided by two, representing the free surface at the top and bottom of the slab model, then, converted to the desired units for comparison. Both single-point energy (i.e., unrelaxed), and geometry-optimized surface energies were calculated, the later with the lattice parameters remaining fixed while atomic positions were allowed to move.

Boehmite Symmetry Considerations

The boehmite structure and atomic positions were modeled based on a neutron diffraction study by Corbato et al.[10] In that study, a variety of space groups were proposed based on the possible arrangement of hydrogen atoms. Here, the energies of three space groups were evaluated: *Cmcm*, $Cmc2_1$, and $P2_1/b$. Results from these calculations are shown in Table S2 and the lower and more similar energies of single unit cell structures with $Cmc2_1$ and $P2_1/b$ symmetries versus *Cmcm* symmetry is consistent with previous studies.[5] As such, bulk incorporation energy calculations were pursued with *Cmcm* symmetry, and surface energy and (near-) surface incorporation energies were pursued with *Cmcm* and $P2_1/b$ symmetries. The latter was used to off-set the formation of a dipole moment associated with some crystallographic terminations of boehmite. It should be noted that space group symmetries were used only to generate atomic positions in the models as calculations were run with P1 symmetry to allow for symmetry breaking due to Cr substitution.

Table S2. Single Unit Cell Calculations for Boehmite with Different Symmetry (i.e., H-positions)

Symmetry System	Opt Level	Total Energy (Ha)	a (Å)	b (Å)	c (Å)	a (deg)	b (deg)	γ (deg)	Vol (Å^3)	Den (g/cm^3)
Boehmite, Cmcm	SPE	-3140.2706	5.7362	12.2336	3.6923	90.0000	90.0000	90.0000	259.1049	3.075
Boehmite, $Cmc2_1$	SPE	-3140.3342	5.7362	12.2336	3.6923	90.0000	90.0000	90.0000	259.1049	3.075
Boehmite, $P2_1/b$	SPE	-3140.3350	5.7362	12.2336	3.6923	90.0000	90.0000	90.0000	259.1049	3.075

Additional Computational Details

The quantum-mechanical code CRYSTAL14[11] was used to perform bulk (and surface) calculations on the Cr-doped boehmite system. In CRYSTAL, the electronic structure of each atom is described by basis sets made up of a linear combination of Gaussian-type functions, referred to as "Atomic Orbitals (AO's)".[11] In turn, the electronic structure of the whole system is described by a linear combination of Bloch functions made up of AO's to generate a "Crystalline Orbital" from which total energies are derived. Calculations were performed using the unrestricted Hartree-Fock (UHF) level of theory that accounts for unpaired spin while calculating exact exchange for electrons in the system. In this study, infinite 3-D periodic models, finite 2-D slab (or surface) models, and single atom ("molecule") calculations were performed to generate the component energies needed to evaluate surface and incorporation energies.

All-electron basis sets were chosen for Al, O, H, and Cr based on previous computational success. Specifically, basis sets for Al, O, and H are referenced to an extensive study on aluminum (oxy-)hydroxide phases by Demichelis et al. using similar computational methods.[5] The basis set for Cr was chosen based on its success in capturing the structure and properties of Cr_2O_3 here and in previous studies.[6] Results from energy and geometry optimization of phases used for basis set testing are provided in Table S1. All single-point energy runs were converged so that changes in energy between consecutive optimization steps were less than $1x10^{-4}$ Ha (or $2.7x10^{-3}$ eV). For atom-only and full-geometry optimizations, where atomic positions or atomic positions and lattice parameters were allowed to optimized, respectively, convergence was achieved when energy differences were less than $1x10^{-5}$ Ha (or $2.7x10^{-4}$ eV) between geometry optimization steps and forces were minimized.

Table. S3 Basis Set Performance Evaluation Calculations for Al_2O_3 and Cr_2O_3 (single unit cells)

Structure	Opt Level	Total Energy (Ha)	a (Å)	b (Å)	c (Å)	a (deg)	b (deg)	γ (deg)	Vol (Å^3)	Den (g/cm^3)
Corundum	SPE	-4254.0475	4.7570	4.7570	12.9877	90.0000	90.0000	120.0000	254.5243	3.991
Al_2O_3	AO	-4254.0476	4.7570	4.7570	12.9877	90.0000	90.0000	120.0000	254.5243	3.991
	FG	-4254.0495	4.7371	4.7371	12.9236	90.0010	90.0010	119.9991	251.1524	4.044
% difference			-0.42	-0.42	-0.49	0.00	0.00	0.00	-1.32	1.33
Eskaolite	SPE	-13869.6344	4.9530	4.9530	13.5884	90.0000	90.0000	120.0000	288.6926	5.241
Cr_2O_3	AO	-13869.6387	4.9530	4.9530	13.5884	90.0000	90.0000	120.0000	288.6926	5.241

	FG	-13869.6629	5.0555	5.0554	13.6845	90.0007	90.0001	119.9996	302.8901	4.995
% difference			2.07	2.07	0.71	0.00	0.00	0.00	4.92	-4.69

SPE = Single-point energy calculations; AO = Atom-only geometry optimizations; FG = full-geometry optimizations

References

(1) *Powder Diffraction File Inorganic and Organic Data Book*; Kabekkodu, S., Ed.; International Center for Diffraction Data: Newtown Square, PA, USA, 2015; Vol. 60.

(2) Larson, A. C.; Dreele, R. B. V. Los Alamos National Laboratory 1994.

(3) Toby, B. H. *J Appl Crystallogr* **2001**, *34*, 210.

(4) Mitchell, D. R. G.; Schaffer, B. *Ultramicroscopy* **2005**, *103*, 319.

(5) Demichelis, R.; Noel, Y.; Ugliengo, P.; Zicovich-Wilson, C. M.; Dovesi, R. *J Phys Chem C* **2011**, *115*, 13107.

(6) Catti, M.; Sandrone, G.; Valerio, G.; Dovesi, R. *J Phys Chem Solids* **1996**, *57*, 1735.

(7) Smith, F. N.; Taylor, C. D.; Um, W.; Kruger, A. A. *Environ Sci Technol* **2015**, *49*, 13699.

(8) Smith, F. N.; Um, W.; Taylor, C. D.; Kim, D. S.; Schweiger, M. J.; Kruger, A. A. *Environ Sci Technol* **2016**, *50*, 5216.

(9) Skomurski, F. N.; Ewing, R. C.; Rohl, A. L.; Gale, J. D.; Becker, U. *Am Mineral* **2006**, *91*, 1761.

(10) Corbato, C. E.; Tettenhorst, R. T.; Christoph, G. G. *Clay Clay Miner* **1985**, *33*, 71.

(11) Dovesi, R.; Orlando, R.; Erba, A.; Zicovich-Wilson, C. M.; Civalleri, B.; Casassa, S.; Maschio, L.; Ferrabone, M.; De La Pierre, M.; D'Arco, P.; Noel, Y.; Causa, M.; Rerat, M.; Kirtman, B. *Int J Quantum Chem* **2014**, *114*, 1287.